Evaluation of the inkjet fluid's performance using the "Cambridge Trimaster" filament stretch and break-up device

D. C. Vadillo[a)]

Department of Chemical Engineering and Biotechnology, University of Cambridge, Cambridge CB2 3RA, United Kingdom

T. R. Tuladhar

Xaar Technology, Cambridge CB4 0XR, United Kingdom

A. C. Mulji

Department of Chemical Engineering and Biotechnology, University of Cambridge, Cambridge CB2 3RA, United Kingdom

S. Jung and S. D. Hoath

Institute for Manufacturing, University of Cambridge, Cambridge CB3 0FS, United Kingdom

M. R. Mackley

Department of Chemical Engineering and Biotechnology, University of Cambridge, Cambridge CB2 3RA, United Kingdom

(Received 6 May 2009; final revision received 15 December 2009; published 18 February 2010)

Synopsis

This paper describes the design and initial results from the "Cambridge Trimaster," a recently developed high speed filament stretch and break-up device that can be used for viscoelastic fluids with shear viscosities as low as 10 mPa s. Extensional viscosity and filament break-up behavior were studied optically using a high speed camera and extensional viscosity values determined for a series of mono-disperse polystyrene solutions up to a weight concentration of 5 wt % were measured as a function of the polymer loading. The transient stretching and break-up profiles recorded with the apparatus were observed and correlated with drop formation for drop-on-demand inkjet printing fluids. This allowed the filament break-up behavior to be ranked in terms of satellite drop and droplet filament behavior. Correlation with previous work on the jetting of similar low viscosity viscoelastic polymer solutions demonstrated the ability of this apparatus to characterize inkjet fluids. © *2010 The Society of Rheology.* [DOI: 10.1122/1.3302451]

[a)]Author to whom correspondence should be addressed; electronic mail: dv244@cam.ac.uk

I. INTRODUCTION

Elongational filament stretching and subsequent capillary thinning of polymer fluid threads are well established experimental methods for exploring extensional viscosity and reviews by McKinley (2005), McKinley and Sridhar (2002), and Bach *et al.* (2003) provide detailed information on both experiments and modeling for a range of polymer systems. In the past, experiments have mostly been conducted at room and elevated temperature for fluid viscosities in the range of 1–50 Pa s [Kolte and Szabo (1999); McKinley and Tripathi (2000); Stelter *et al.* (2000)]. Fluids with a viscosity between 2 and 10 mPa s and with a break-up time after piston cessation of motion down to 30 ms have also been reported by Rodd *et al.* (2005).

Several devices have been built in order to investigate the elongation properties of viscoelastic fluids and the apparatus used for such application function by stretching a small amount of fluid attached between two identical pistons. Two different methods have been used to measure the transient elongational viscosity: (a) filament stretching and (b) filament thinning. In terms of filament stretching apparatus, the evolution of filament diameter with time can yield the apparent elongational viscosity of the fluid, provided a mass or force transducer is included in the apparatus. In an early apparatus, introduced by Matta and Tytus (1990), a top piston was kept fixed and a second piston of known mass moved downward under gravity. In this case, the filament thinned due to the motion of the mass and the Hencky strain was calculated directly from the displacement of the bottom piston. Sridhar (1990) and Sridhar *et al.* (1991) introduced a mechanically driven piston where an exponential stretch could be applied to the filament. This experimental set-up included a force transducer, connected to the fixed piston, to measure the transient load. Orr and Sridhar (1999) introduced a mechanical system where both pistons moved in opposite directions with the benefit that the central filament position remained constant, thereby making filament diameter measurements easier to follow with greater accuracy. This feature can however increase both the size and complexity of the apparatus. Bach *et al.* (2002) used a double piston device where a laser controlled the mid-filament diameter to ensure a constant stretch rate and further developed their apparatus for elevated temperature measurements [Bach *et al.* (2003)].

In terms of filament thinning, Bazilevsky *et al.* (1990) invented a capillary thinning device ("liquid filament microrheometer") for measuring the diameter decay of a prestretched polymer thread. The device imposed an initial rapid extensional step strain using the action of a spring on one piston that created a liquid bridge, which then subsequently self-thinned under the action of viscous, elastic, and capillary forces. The transient Hencky strain was calculated by the rate of thinning of the mid-filament diameter with time. Experimental data were obtained by Liang and Mackley (1994) using Bazilevsky's device. Anna *et al.* (1999) and Anna and McKinley (2001) further developed variants of the Bazilevsky's apparatus and a "CaBER" filament thinning apparatus is now sold by Thermo scientific (http://www.thermo.com/com/cda/product/detail/) allowing low viscosity fluid to be considered.

Recently, Tuladhar and Mackley (2008) showed that the Cambridge multipass rheometer (MPR) [Mackley *et al.* (1995)] can be modified to perform high speed filament stretching and thinning experiments. The MPR was modified from its normal configuration and the two mutually opposed servo-hydraulically driven pistons were used to stretch a filament at high speed, while leaving the center of the filament in the same position within the laboratory frame of reference. This enabled a high speed camera to be positioned at the center and follow the progressive thinning of the thread during and after a controlled stretch deformation. Piston speeds of up to 300 mm/s were achieved and fluid

viscosities of order 10 mPa s could be measured. The MPR filament stretching and thinning apparatus performed the required function; however, the costly and large servo-hydraulic drive aspect of the apparatus was an unnecessary complication. A smaller and simpler device called the "Cambridge Trimaster" has been developed and is described in this paper. This apparatus was specially designed to characterize low viscosity inkjet fluids where both the capillary thinning and break-up could be observed for thinning and break-up times down to of order 5 ms.

II. EXPERIMENTAL APPARATUS

The key design feature of the Cambridge Trimaster (shown in Fig. 1, both as a schematic diagram and as a photograph of the apparatus) retains the MPR concept of maintaining the center of the thread in one position. This was achieved by having two pistons attached to a band and a slider, as shown schematically in Fig. 1(a). Table I describes the differences in response between the MPR filament stretching experiments carried out by Tuladhar and Mackley (2008) using a MPR and the developed Cambridge Trimaster apparatus. Overall performance is similar, however, the Trimaster does not utilize the complexity of servo-hydraulicly driven pistons used with the MPR. The rotation of a stepper motor drive causes both the upper and lower pistons to move in synchronization with each other. This mechanical system overcame the complication of servo-hydraulic control and a low cost stepper motor (200 steps/revolution), combined with a pulley of diameter 10 mm, was capable of reaching a relative piston velocity $2V_p$ of 1 m/s. A micro-stepping card was added to improve the performance of the system, achieving an adjustable number of steps per revolution between 600 and 50 000, allowing a smoother displacement [Fig. 1(c)]. That enabled a sample stretch distance from 10 μm to 10 cm on each side at a relative velocity from 10 mm/s to 1 m/s. Figure 1(c) shows the camera recorded piston displacement as a function of time for different piston velocities. The 10 and 100 mm/s piston velocities show a clear linear response followed by a rapid deceleration and fixed displacement. This motion represents a desired experimental boundary condition. The 500 mm/s motion is less satisfactory, as the data show a good initial linear response, however, there is a transient displacement on the cessation of motion. The piston oscillation on the cessation of motion seen in Fig. 1(c) for the high piston speed (oscillation frequency between 100 and 200 Hz) was due to the inertial response of the system and the micro-stepping of the electronic control card. Various attempts have been made to minimize this issue and are currently being addressed for future machines.

Filament stretching experiments were performed at ambient temperature by placing the sample fluid between the two pistons of diameter of D_0 (1.2 mm in this study). The sample was stretched from an initial separation distance L_0 (600 ± 10 μm in the present work) up to a set distance L (between 1400 and 2200 ± 10 μm in the present work) as shown in Fig. 1(d). The filament aspect ratio is defined as $2L/D_0$. In the filament stretching and thinning mechanism, viscous forces tend to stabilize the cylindrical shape of the filament whereas gravity can drag the fluid below the mid-filament. The competition between gravitational and viscous forces can be estimated by the ratio of the Bond number to the capillary number, $B_o/Ca = \rho g D_0/2\eta_0\dot{\varepsilon}$, where ρ is the fluid density, g is the gravitational constant, and $\dot{\varepsilon}$ is the strain rate defined as $2V_p/L_0$. In the present work, Bo/Ca has been founded to be lower than 0.28 ensuring a viscous dominated thinning mechanism.

The filament stretching and thinning profiles were observed using a high speed camera (Photron Fastcam 1024 PCI), synchronized to the initial motion of the pistons, and

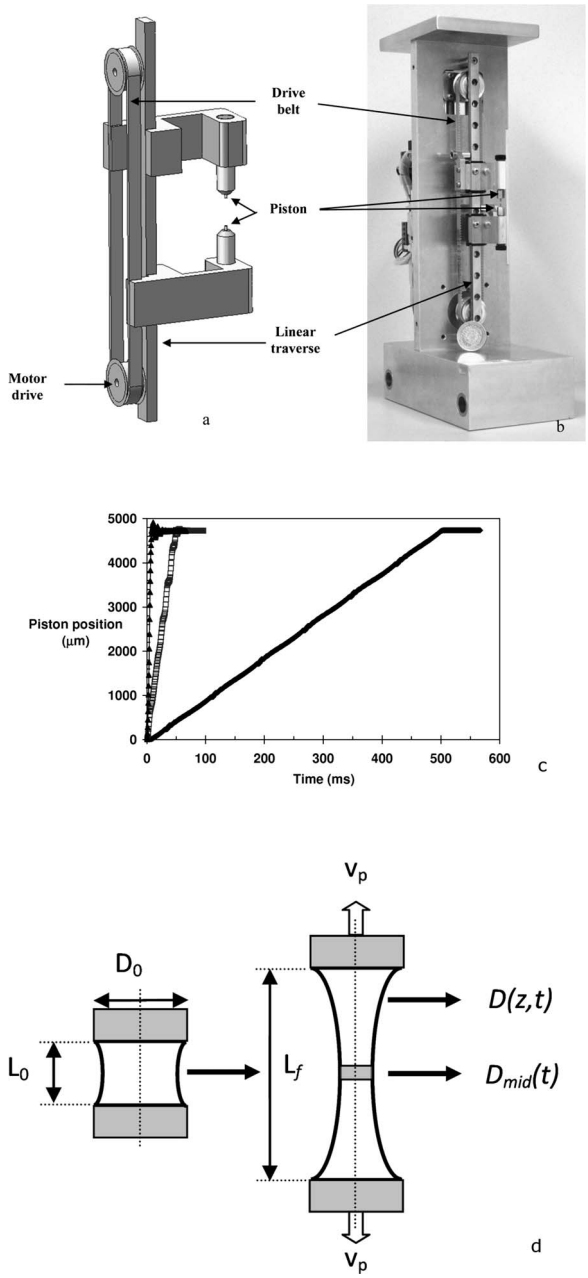

FIG. 1. (a) Schematic and (b) photograph of the Cambridge Trimaster. (c) Piston motion at different velocities with (♦) 10 mm/s, (□) 100 mm/s, and (▲) 500 mm/s. (d) Description of the geometrical parameters of the system.

photographs of the whole filament profile as a function of time were obtained. A photograph of the "Cambridge Trimaster" together with the associated optics is shown in Fig. 2. The camera can record 1024×1024 pixel pictures at 1000 frames per second and a binning option enables pictures to be recorded at up to 100 000 frames per second but at a reduced resolution (32×32 pixels). The shutter time can also be reduced to 3 μs and

TABLE I. Point by point comparison of the main features of the MPR and the Cambridge Trimaster.

	MPR	Trimaster (II)
Piston movement	Two independent servo-hydraulic controlled motors	Single stepper motor and pulley system
Initial stretch velocity	$\leq$300 mm/s	Current setting: $\leq$1000 mm/s
Total displacement	$\leq$30 mm on each side	$\leq$100 mm on each side
Minimum step size	0.05 mm	$\sim$2 μm/step (50 000 steps/rev)
Resolution: Plate oscillations when piston stops	$\pm$0.1 mm for $<$10 ms	$\pm$0.10 mm for $<$3 ms at 500 mm/s speed
Advantage	Smaller step size, multi-purpose	Cost, flexible speed and step size, portable, apparatus size
Disadvantage	Cost, size	

the light was provided by a continuous fiber optic. The filament thinning measurement, as well as the filament break-up behavior, was obtained using automatic image treatment specifically developed and included within the "Cambridge Trimaster" software suite. The standard operating conditions used in this paper were frame rates of 6000 and 27 000 fps with a shutter time of 3 μs due to the very short time scale associated with the break-up mechanism of low viscosity viscoelastic fluid. Spatial resolution for the experiments described in this paper was of order 5 μm which was sufficient to ensure accurate measurements. Resolution can be improved with enhanced camera and light capabilities. Line scanning devices of the type used in the CaBER can achieve of order 2.5 μm depending on the system used.

The fluids that were used were a series of mono-disperse polystyrene (PS) with a molecular weight of 110 kg/mol (PS110) at different concentrations (0, 0.2, 0.5, 1, 2.5, and 5 wt %, respectively) dissolved in diethyl phthalate (DEP). The surface tension was measured using a "Wilhelmy plate" method and a "SITA, pro-line t15" bubble pressure tensiometer. A typical value of 37 mN/m was obtained for both the pure DEP and a mixture of 5 wt % PS100 in DEP. The viscosities η_0 of the solutions were determined from low frequency complex viscosity η^* measurements, where η_0 covers a range of between 10 and 73 mPa s (Table II). The high frequency linear viscoelastic properties of

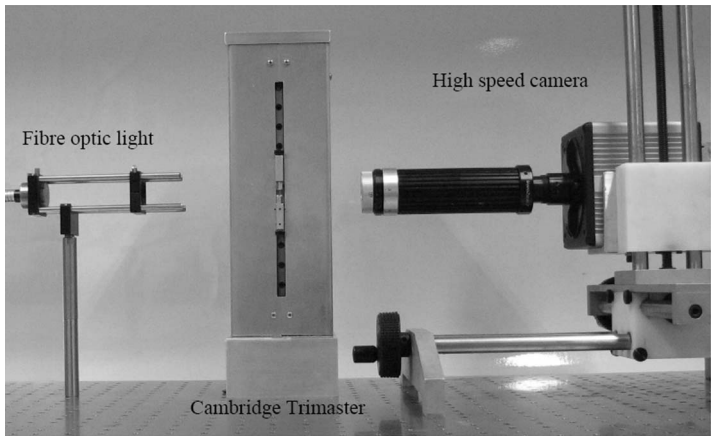

FIG. 2. Photograph showing the Trimaster and optical assembly that includes back illumination and a high speed camera.

TABLE II. Physical properties of the sample of DEP+PS110. Complex viscosity data given in table were obtained from rheological data presented in the Appendix.

Polymer concentration (wt %)	Complex viscosity η^* (mPa s)	c/c^*	Surface tension σ (mN/m)	Density ρ (kg/m^3)
0	10	0	37	1120
0.2	10.8	0.083	37	1120
0.5	13.7	0.208	37	1120
1	15.3	0.417	37	1120
2.5	27.6	1.041	37	1120
5	65.4	2.08	37	1120

these fluids were measured using the high frequency rheometer "piezo axial vibrator." Details of this apparatus are not presented here but have been reported elsewhere [Groß *et al.* (2002); Crassous *et al.* (2005)]. Results are given in the Appendix. Finally, the critical polymer overlap concentration c^* was determined using $c^*=0.77/[\eta]$, where $[\eta]$ is intrinsic viscosity [Graessley (1980)]. Using the Mark–Houwink–Sakurada equation $[\eta]=K_{[\eta]}M^{\gamma}$, where $K[\eta]=8.1\times10^{-3}$ and $\gamma=0.704$, c^* of 2.40% is obtained for 110 000 g/mol PS for DEP-PS solution [Clasen *et al.* (2006)].

III. RESULTS AND DISCUSSION

A. Extensional viscosity measurements

It is well established that the addition of a small amount of polymer can significantly influence the extensional rheology of a fluid [see, for example, Anna and McKinley (2001); Tuladhar and Mackley (2008)]. The addition of polymer increases the viscosity of the fluid and also the viscoelastic behavior develops, which can strongly affect filament thinning and break-up mechanisms. Figure 3 presents a series of photographs of the filament stretching experiments performed from an initial length of 600 μm to a final stretching distance of 1400 μm at a piston relative velocity of 150 mm/s for a series of mono-disperse PS (110 000 g/mol) solutions dissolved in DEP and recorded at a frame rate of 6000 fps with a picture size of 256×512 pixels (spatial resolution is 5.5 μm per pixel). The initial cylindrical form of the filament is ensured by an initial filament length L_0 smaller than the capillary L_{cap}, defined as $L_{cap}=(\sigma/\rho L_0)^{1/2}$ and estimated at 1.7 mm here [Rodd *et al.* (2005)]. The initial and final aspect ratios of the filament were 1 and 2.3, respectively. Figure 3 shows that at 5.3 ms, the initial form of the filaments is similar. In principle, extensional viscosity data could be obtained from this early stage deformation if a transient force measurement was simultaneously obtained as in the filament stretching experiments performed, for example, by Matta and Tytus (1990) or Spiegelberg *et al.* (1996). The "Cambridge Trimaster" is not fitted with force measuring capacity and therefore filament capillary thinning observed after piston cessation was used.

Once the pistons had stopped moving (t=5.3 ms), the central part of the filament had the general form of a cylinder. At this point, surface tension σ causes the filament to thin and the fluid viscosity η acts against this process. With the addition of a small amount of polymer (up to 0.5 wt %), the filament thinning process slowed down and the filament lifetime increased. For higher concentrations of polymer, both the elastic modulus G' and the viscous modulus G'' increased (see the Appendix for rheological data on fluids) and this resulted in a longer break-up times.

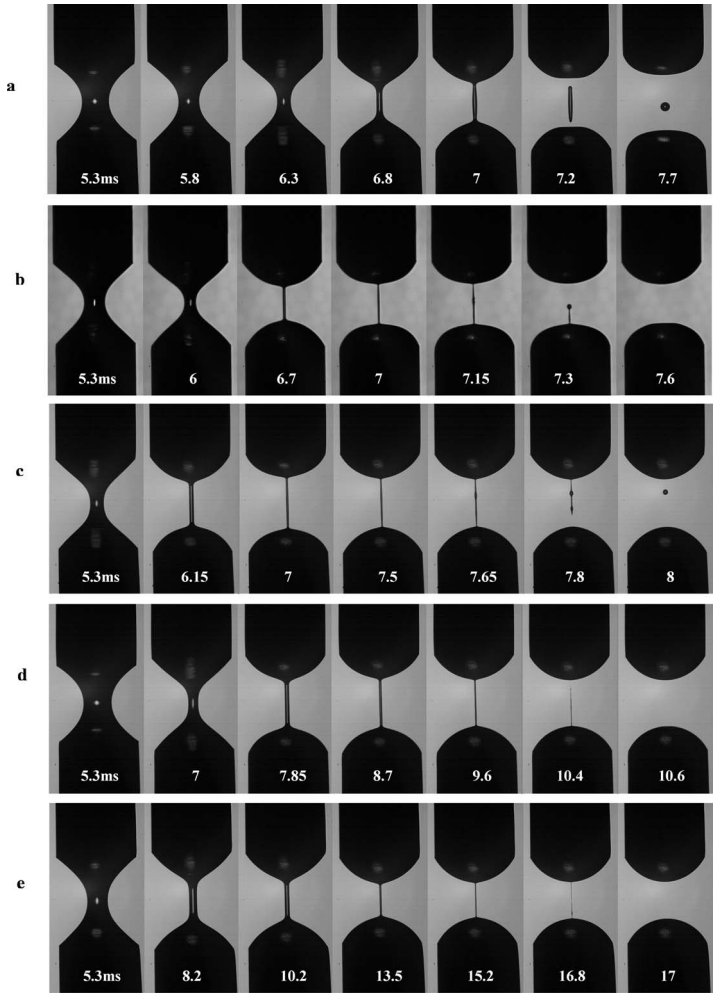

FIG. 3. Photograph of the filament break-up captured with the Trimaster in the extensional viscometer modes of (a) DEP, (b) DEP+0.2 wt % PS110, (c) DEP+0.5 wt % PS110, (d) DEP+1 wt % PS110, and (e) DEP +2.5 wt % PS110. Initial gap size: 0.6 mm; stretching distance: 0.8 mm; stretching velocity: 150 mm/s. Piston diameter: 1.2 mm.

High speed photographic observation of the filament transient profiles showed the influence of the addition of polymer. Three different forms of filament behavior were identified and are shown in Fig. 3. The first Newtonian form is shown in Fig. 3(a) for pure DEP (low viscous Newtonian fluid). Initially, the filament remains essentially in a cylindrical form up to t=6.8 ms (1.5 ms after the stretching process stopped), subsequently the filament became non-uniform where the ends thinned faster than in the mid-filament. Finally, the filament exhibited clear top and bottom end pinching and break-up at t=7.2 ms, resulting in the formation of a central droplet [Fig. 3(a)]. This behavior is different for cases of higher viscosity Newtonian fluids reported by Liang and Mackley (1994) and Anna and McKinley (2001) where the central filament decades without end pinching.

The other extreme case was the thinning mechanism of a highly viscoelastic fluid shown in Figs. 3(d) and 3(e), where the elasticity controls the thinning process [Liang and

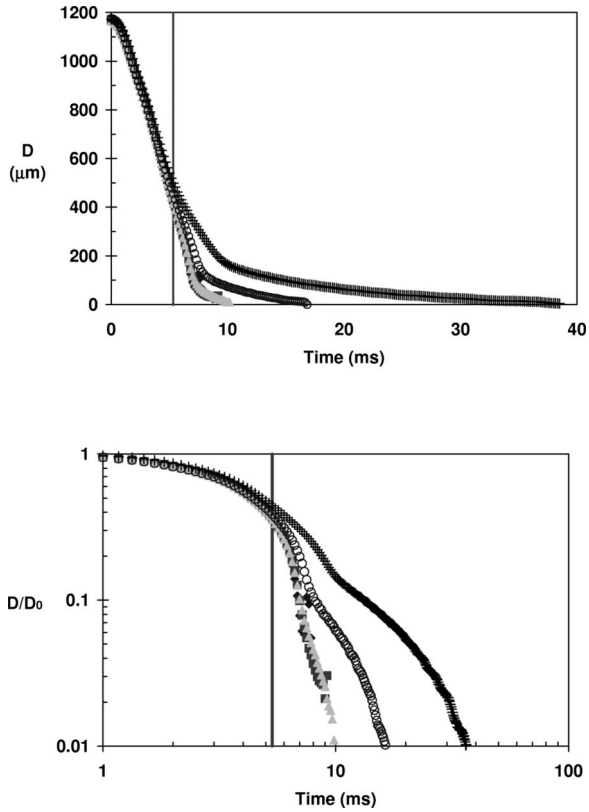

FIG. 4. (a) Evolution of the mid-filament of the photograph of Fig. 2. (♦) DEP, (■) DEP−0.5 wt % PS, (▲) DEP−1 wt % PS, (○) DEP−2.5 wt % PS, (+) DEP−5 wt % PS, (−) piston cessation of motion. (b) Evolution of the normalized mid-filament of the photograph of Fig. 2. (♦) DEP, (■) DEP−0.5 wt % PS, (▲) DEP−1 wt % PS, (○) DEP−2.5 wt % PS, (+) DEP−5 wt % PS, (−) piston cessation of motion.

Mackley (1994); Anna and McKinley (2001)]. The addition of polymer prevented the formation of a central drop and the development of a long lasting uniform filament was observed with no one identifiable break-up point.

An intermediate type of filament behavior shown in Figs. 3(b) and 3(c) was observed between the two extreme cases. During the filament relaxation, one or several small droplets were formed along the thread due to Rayleigh instability, connected by a very thin filament. The break-up occurred along the thread but no exact position was clearly identifiable.

Figure 4 shows the time evolution of the mid-filament width for the experimental conditions presented in Fig. 3. It can be seen in Fig. 4 that the deformation is similar up to the piston cessation that occurs at 5.3 ms. Once the piston has stopped (t=5.3 ms), the mid-filament diameter was approximately 435 μm for all of the experiments. From this point, the filament thinned under the effect of the capillary forces with a different characteristic, depending on the nature of the sample. The filament diameter of the Newtonian sample (DEP) decreased linearly with time, as predicted by the literature [McKinley (2005); Bazilevsky *et al.* (1990); Kolte and Szabo (1999); Entov and Hinch (1997); Liang and Mackley (1994)]. The evolution of the mid-filament D_{mid} for such a case is given by the following equation:

$$D_{mid}(t) = \alpha\left(\frac{2\sigma}{\eta_0}\right)(t_{bu} - t), \tag{1}$$

where σ is the surface tension of the fluid, η_0 is the viscosity of the fluid, t_{bu} is the break-up time defined from the instant of the piston stopping, and with α a coefficient fitted here at 0.0272. This coefficient is not constant but depends on the nature of the test solution. For example, McKinley and Tripathi (2000) showed that this description agreed well in the case of experiments with a high viscous Newtonian fluid (α=0.0709).

As the amount of polymer was increased, the thinning diameter decreased exponentially. The addition of a low concentration of polymer (<1 wt %) slightly changed the filament thinning profile just before the break-up. This implies that the <1 wt % fluids behaved essentially in a Newtonian way during the major part of the thinning with a dominance of the polymer effect toward the end. For higher polymer concentrations, the early stage of the thinning was also dominated by the Newtonian nature of the solvent, but at later stage, the mid-filament width exhibited an exponential decrease with time as a result of the polymer influencing the deformation (Fig. 4). Such behavior has been theoretically predicted in the literature [Bazilevsky *et al.* (1990); Renardy (1994, 1995); Brenner *et al.* (1996); Bazilevsky (1997); Eggers (1997); Entov and Hinch (1997)] and experimentally demonstrated [Liang and Mackley (1994); Anna and McKinley (2001)]. Experiments on low viscosity polymer solutions [Tuladhar and Mackley (2008)] and high viscosity polymer solutions [Bazilevsky *et al.* (1990); Kolte and Szabo (1999); McKinley (2005); Ma *et al.* (2008)] have also shown a similar exponential behavior during the filament thinning mechanism.

An apparent extensional viscosity η_E for an axial cylindrical filament, thinning under the action of the capillary pressure, can be derived from the filament diameter thinning process using a model developed by McKinley and Tripathi (2000)

$$\eta_E = (2X - 1)\frac{\sigma}{-dD_{mid}(t)/dt}, \tag{2}$$

where D_{mid} is the mid-filament diameter and X is a coefficient, which takes into account how the shape of the filament deviates from a uniform cylindrical thread due to the inertia and gravity. In the case of a highly viscous Newtonian fluid, McKinley and Tripathi (2000) reported X=0.7127 as the most appropriate coefficient. The X coefficient has also been found to be necessary for low viscosity Newtonian and viscoelastic fluids [Tuladhar and Mackley (2008)], as shown by an experimental study using a different filament stretcher (multi-pass rheometer) using similar fluids as investigated here (PS Mw =195 kg/mol, concentration up to 5 wt % dissolved in DEP). These results have been confirmed by numerical simulation, where X ranges from 0.53 and 0.71 for inertia and inertia-less Newtonian viscous cylindrical filament formations, respectively [Brenner *et al.* (1996); Eggers (1997); Papageorgiou (1995)].

The apparent extensional viscosity of the sample presented in Fig. 3 has been estimated using Eq. (2) and is reported in Fig. 5. This figure presents the evolution of the transient Trouton ratio (η_E/η_0) as a function of the filament thinning Hencky strain ($\varepsilon = 2\ln(D_0/D(t))$) for the PS110 dissolved in DEP after the piston has stopped. The maximum Hencky strain ε_{max} that can be recorded depends on the spatial resolution of the recorded picture. In these experiments, the spatial definition of the captured images was 5.6 μm which corresponded to a maximal measurable filament thinning Hencky strain ε_{max} defined by Anna and McKinley (2001) of

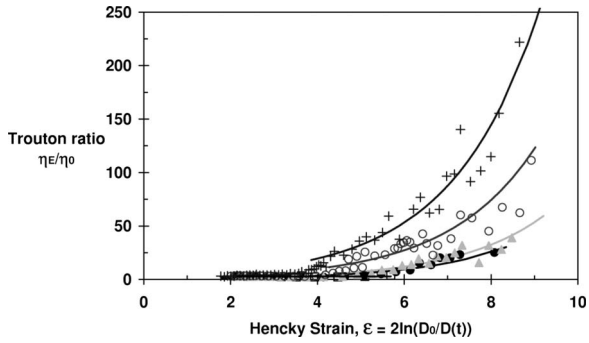

FIG. 5. Transient extensional rheology of DEP solutions as a function of relaxation Hencky strain for different PS concentrations. Initial distance 0.6 mm, final distance: 1.4 mm, piston velocity: 150 mm/s. The lines are obtained from the exponential fitting of the evolution of the thinning of the diameter. The geometrical factor "X" is fitted using the experimental data at low Hencky strain. (♦) DEP, (■) DEP−0.5 wt % PS, (▲) DEP −1 wt % PS, (○) DEP−2.5 wt % PS, (+) DEP−5 wt % PS.

$$\varepsilon_{\max} = 2\ln\left(\frac{1.2e^{-3}}{5.6e^{-6}}\right) = 10.7. \tag{3}$$

At such a Hencky strain and high strain rate, polymer molecules can be expected to be fully extended. The maximum extension for the polymer molecules used in this study was of the order of $n^{1/2} \approx 30$ ($\varepsilon \approx 3.4$), where n is the number of random coil repeat units and $\varepsilon_{\max} = 10.7$ corresponds to a linear extension of order of 44 000.

The approximate derivative of the mid-filament diameter was obtained by the calculation of the decrease of the mid-filament between two recorded frames (symbols on the figure). Thus, the exact derivate $dD_{mid}(t)/dt$ becomes $[D_{mid}(t_i) - D_{mid}(t_{i-1})]/(t_i - t_{i-1})$, where i is the current frame number. An exponential fitting was also used and allowed a smoother estimation of the transient Hencky strain (solid line). Theoretically, the value of the extensional viscosity, η_E, is 3 times the shear viscosity, η_0, for a Newtonian fluid. Consequently, X was adjusted by fitting Eq. (2) in order to obtain a Trouton ratio equal to 3 at low Hencky strain for all experiments. For the five cases considered in Fig. 4, the X coefficient was fitted at 0.573, 0.583, 0.6, 0.68, and 0.78 for 0, 0.5, 1, 2.5, and 5 wt % polymer concentrations, respectively. With increasing polymer concentration, the double curvature of the filament reduced and the Ohnesorge number ($Oh = \eta/(\rho D_0 \sigma)^{1/2}$), which can represent the ratio between visco-capillary ($t_v \approx \eta_0 D_0/\sigma$) and the inertio-capillary ($t_i \approx (\rho D_0^3/\sigma)^{1/2}$) processes [Rodd *et al.* (2005)], increased resulting in the filament shape becoming more cylindrical (perfect cylinder corresponds to X = 1). The fitted values of X were similar to the results reported previously by Tuladhar and Mackley (2008), although the filament aspect ratio was different [2.3 in the present work, 6 in Tuladhar and Mackley (2008)], with the exception of the 5 wt % polymer concentration. The shape of the filament was influenced by the stretching distance, as demonstrated in Fig. 5 with a subsequent consequence on X value.

The maximum extensional viscosity was found to be a non-linear function of the polymer concentration (Fig. 5), which was previously reported by Tuladhar and Mackley (2008). For the five mixtures in the present study, the maximum Trouton ratio $\eta_{E\,max}/\eta_0$ before the break-up increased with polymer concentration and was measured to be 3, 30, 60, 123, and 267 for 0, 0.5, 1, 2.5, and 5 wt % PS110 dissolved in DEP, respectively (Fig. 5).

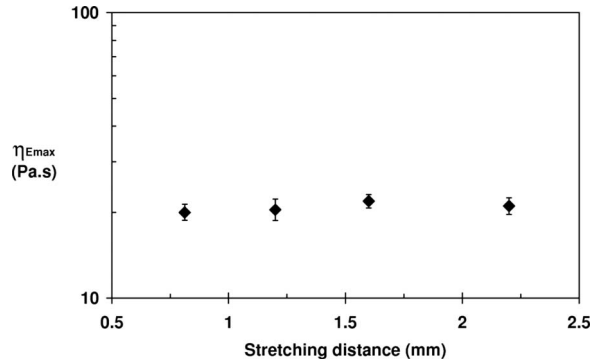

FIG. 6. The maximum extensional viscosity $\eta_{E\,max}$ of DEP−5 wt % PS110 as a function of relaxation Hencky strain for four different stretching distances. Initial distance 0.6 mm; piston relative velocity: 150 mm/s.

The filament thinning experiments were repeated for 5 wt % of PS110 in DEP using four different final aspect ratios (from 2.33 up to 4.66). The initial piston separation and piston relative speed were kept constant at 0.6 mm and 150 mm/s, respectively, for all experiments. Within the specified stretching range, X was fitted as described previously and increased up to 0.93 for a final piston distance of 2.8 mm, indicating that the aspect ratio of the filament influences the filament shape. However, the measured maximum extensional viscosity $\eta_{E\,max}$ was independent of the stretching distance ($\eta_{E\,max} = 20.9 \pm 1.4$ mPa s) as presented in Fig. 6. Other authors have reported a similar result in the case of glass-fiber suspensions [Weinberger and Goddard (1974)] and of carbon nanotubes [Ma *et al.* (2008)]. For those studies, the authors believe that the polymer molecules are fully stretched and aligned within the flow during the stretching mechanism without further subsequent influence during the filament thinning process.

B. Filament break-up and inkjet printing

By operating the Cambridge Trimaster under slightly different conditions to those described in the previous section, namely, using a larger total displacement of the piston, filament break-up was observed and linked to the inkjet performance. Figure 7 shows the way in which the addition of polymer affects the break-up of the filament formed, with a separation velocity of 150 mm/s, an initial plate separation $L_0 = 0.6$ mm to a final distance of $L_f = 2.2$ mm corresponding to a filament stretch strain rate $\dot{\varepsilon} = 250\ s^{-1}$, and a final filament stretching Hencky strain of $\varepsilon_L = \ln(L_f/L_0) \approx 1.3$. As previously, the fluid used here is a series of DEP+PS110 at different weight concentrations (from 0 up to 5 wt %) and captured at a frequency of 6000 fps. Under these experimental conditions, several differences appeared in comparison to Fig. 3, even if the overall description obtained previously remains the same. The main observations made from Fig. 7 are the following:

(a) Newtonian case [Fig. 7(a)]. The liquid bridge of pure DEP exhibited a clear symmetrical top and bottom pinch-off, with the formation of a central satellite.
(b) Slightly viscoelastic behavior [Fig. 7(b)]. The addition of a very small amount of polymer again exhibited the development of a thread between the droplet and the piston. The filament thins before the break-up and this allows Rayleigh instabilities to appear. Subsequently, the filament loses its symmetry and forms satellite drops even if it ends pinching and a unique drop is formed.

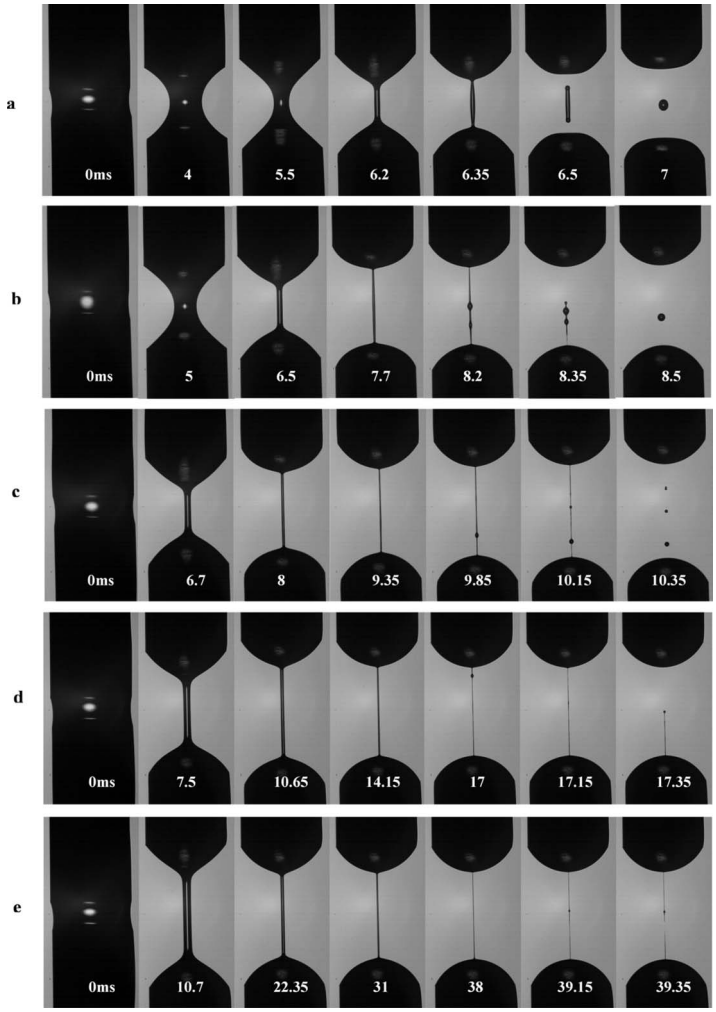

FIG. 7. Photograph of the filament break-up captured with the Trimaster in the filament break-up mode of (a) DEP, (b) DEP+0.5 wt % PS110, (c) DEP+1 wt % PS110, (d) DEP+2.5 wt % PS110, (e) DEP+5 wt % PS110. Initial gap size: 0.6 mm; stretching distance: 1.6 mm; stretching velocity: 150 mm/s. Piston diameter: 1.2 mm.

(c) Intermediate viscoelastic behavior [Fig. 7(c)]. Slow development in viscoelasticity from the case (b) with subsequent influence on the filament break-up mechanism; the filament becomes thinner and the Rayleigh instabilities lead to the break-up of the filament on micro-drops.
(d) High viscoelastic behavior [Fig. 7(d)]. Surface tension is dominated by the viscoelasticity of the fluid leading to the dissipation of the micro-drops. The filament is more stable and longer lasting, resulting in an exponential thinning process.
(e) Higher viscoelastic behavior. The level of elasticity of the fluid is again increased, resulting in an enhancement of the mechanism observed in (d).

Deviation from the Newtonian case can be identified for low polymer concentration addition using an enhanced photographic frame rate. Figure 8 shows a polymer concentration intermediate between Figs. 7(a) and 7(b) where at the previous frame rate of 6000

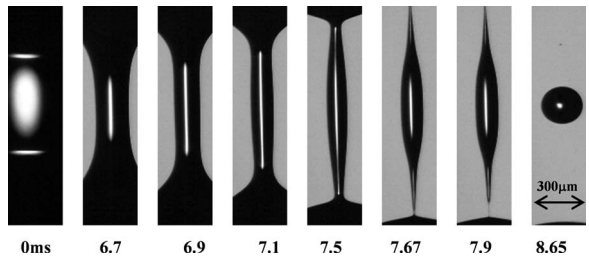

FIG. 8. Photograph of the filament breaks up captured with the Trimaster in the filament break-up mode of DEP+0.2 wt % PS110 (27 000 pictures per second, exposure time 3 μs). Initial gap size: 0.6 mm, stretching distance: 1.6 mm, stretching velocity: 150 mm/s.

fps, break-up would look similar to the Newtonian case. At 27 000 fps, Fig. 8 reveals a fine tail between the stationary plates and the central filament; this feature is important in term of drop-on-demand (DOD) drop break-up mechanisms. In addition, the final break-up time is influenced by the formation of the tail with, in this case, an increase to 8 ms from the Newtonian case of 6.4 ms whereas the viscosity of the two fluids is similar.

IV. DISCUSSION

A. Inkjet printing

The filament break-up process of a fluid is relevant to the inkjet printing, particularly in the continuous inkjet and DOD processes. The fluid volume and velocity, the thread aspect ratio, and equally the fluid rheology control the subsequent drop formation mechanism [Dong *et al.* (2006); Jang *et al.* (2009)]. Figure 9 schematically summarizes the drop formation process for DOD and the effect of polymer addition on DOD inkjet printing. The initial fluid release results in the formation of the cylinder of fluid [Figs. 9(a) and 9(b)], which quickly thins to become conical [Hutchings *et al.* (2007)] under stretching due to capillary force actions and the velocity gradient between the main droplet and the nozzle plate. From this point, three different paths are possible depending on the degree of viscoelasticity of the fluid.

Path 1 corresponds to the Newtonian case where the thread exhibits a clear break-up at the nozzle plate [Fig. 9(c)] and where the filament can subsequently either (i) retract faster than the thinning process [Fig. 9(d)] and form a unique drop [Fig. 9(e)], (ii) develop a second break-up close to the main droplet [Fig. 9(f)] and form a main drop followed by a satellite [Fig. 9(g)], or (iii) exhibit the development of Rayleigh instabilities [Fig. 9(h)] and form a main drop followed by multiple satellites [Fig. 9(i)]. Path 2 considers the case of an intermediate viscoelastic fluid. For a free surface viscoelastic flow, the viscoelasticity level of the fluid can be characterized by the Deborah number ($De=\lambda t_r$), which is the ratio between a fluid relaxation time λ due to polymer addition and the Rayleigh time scale for inertia-capillary break-up of an inviscid jet $t_R=(\rho R_0^3/\sigma)^{1/2}$ estimated here at 2.65 ms and where R_0 is equal to $D_0/2$ [McKinley (2005)]. This causes a thin longer lasting tail between the filament and the nozzle to form [Fig. 9(j)], resulting in an increase of the break-up time at the nozzle, with a subsequent further stretch of the filament [Fig. 9(k)]. The filament can either (i) retract faster than the thinning process and merge into the main drop [Fig. 9(l)] or (ii) exhibit the development of Rayleigh instabilities and form a main drop followed by multiple satellites [Fig. 9(m)].

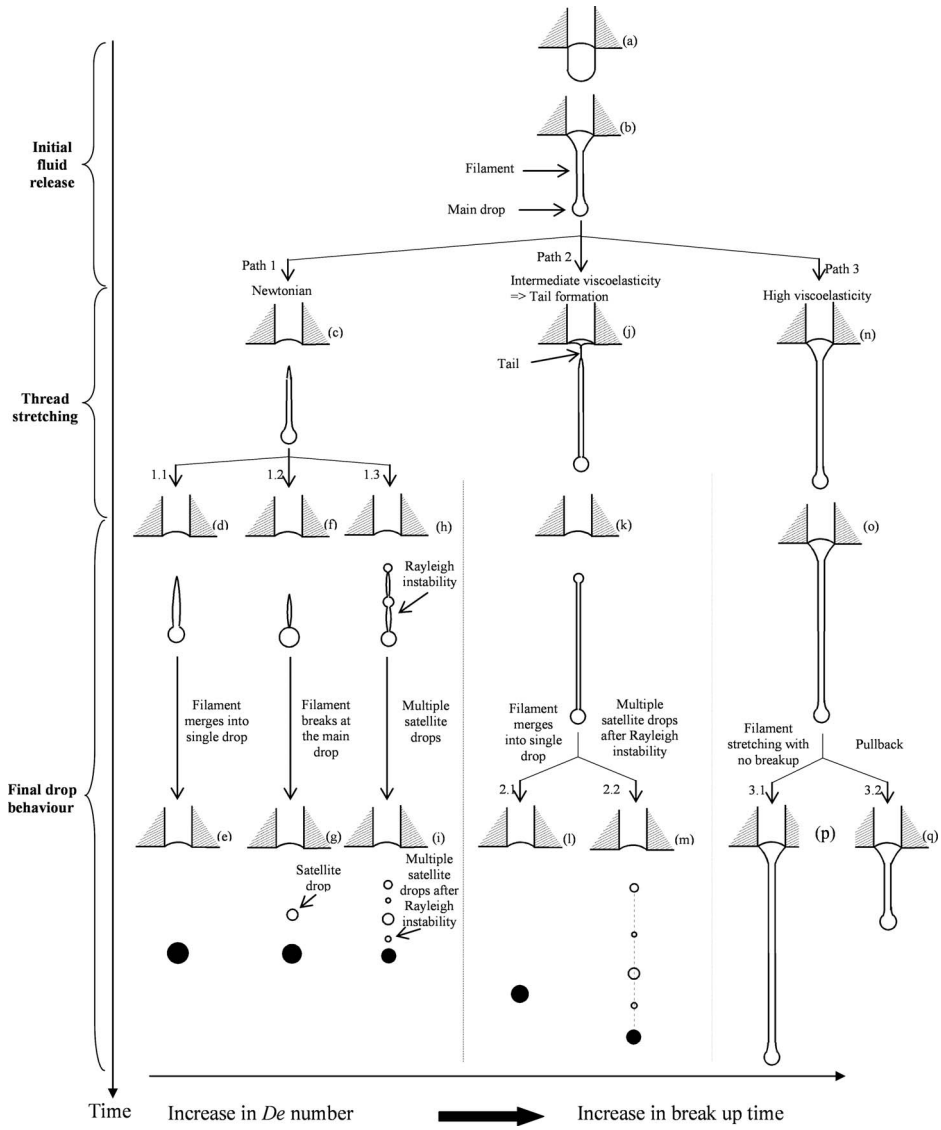

FIG. 9. Schematic of inkjet break-up. The time direction is from the top to the bottom. (a) and (b) are common to all drop ejection. Three paths are shown. Path 1 [from (c) to (i)]: Newtonian case: formation of a unique drop, a main drop followed by a unique satellite or a main drop followed by multiples satellites. Path 2 [from (j) to (m)]: intermediate viscoelasticity: formation of a thin ligament which increasing the break-up resulting on the formation of a unique drop or a main drop followed by multiples satellites. Path 3 [from (n) to (q)]: high viscoelastic configuration: the thread stretches without any break-up and may be pulled back into the printhead.

Path 3 presents the high viscoelasticity configuration (higher De number) where the fluid keeps stretching without any break-up [Fig. 9(p)] and may be pulled back into the printhead [Fig. 9(q)].

B. Linking the Cambridge Trimaster to inkjet performance

The combination of the fast filament stretching experiments over a very short distance performed by the Cambridge Trimaster allows the filament break-up during drop genera-

tion to be mimicked. Typically, the Trimaster allows a fast motion up to 1 m/s over a distance of order 0.8 mm corresponding to a final filament stretching strain rate of order $\dot{\varepsilon} = 1250\ \text{s}^{-1}$. The initial fluid diameter was 1.2 mm and after piston cessation, the central filament has a typical diameter of 0.4mm [see Fig. 4(a)] which corresponds to a maximum filament stretching Hencky strain $\varepsilon_{\max}$ of order 2.2. Further capillary thinning occurs after the cessation of piston motion resulting in additional straining. Here, the central filament diameter may change from say 0.4 mm to the optical resolution of 5 μm resulting in a further relaxation Hencky strain of 8.8.

In the DOD process, the typical drop velocity is about 6 m/s with an initial nozzle size of 50 μm and a spatial resolution of the optical system about 2 μm. This corresponds to a filament stretching strain rate $\dot{\varepsilon}$ of order of 3000 s^{-1} and a maximum filament thinning Hencky strain $\varepsilon_{\max}$ of order 6.

The Ohnesorge number between the drop generation process and the Cambridge Trimaster experiment can be maintained, as well as the filament aspect ratio and the fluid relaxation time. The pictures recorded by high speed camera (Figs. 3, 7, and 8) demonstrate significant similarities with the transient profiles observed during drop generation [Bazilevsky *et al.* (2005); Hoath *et al.* (2009)].

Many of the terms used in inkjet fluid drop formation research are either loosely or ill-defined. In an attempt to standardize the terminology for the sake of clarity, Fig. 10 explicitly points out what each term refers to in the filament stretching experiments using the Cambridge Trimaster in comparison to the DOD process. These terms will be used in subsequent description of the DOD and filament break-up experiments.

The different break-up profiles recorded by the Cambridge Trimaster allow a visual investigation of the viscoelasticity of the fluid and then the classification of the fluids "jettability." Direct comparison between Cambridge Trimaster break-up and DOD behavior is illustrated in Fig. 10. Figure 10(a) shows the point of the break-up for a mildly viscoelastic fluid observed using the Cambridge Trimaster for a specific piston relative velocity of 150 mm/s, an initial gap size of 600 μm, and a stretching distance of 1600 μm. Under those experimental conditions, a central filament is formed together with two fine connecting tails. Figure 10(b) shows photograph of a DOD drop formation again for a mildly viscoelastic fluid. The stationary nozzle plate is at the top of the photograph and again a thin tail can be seen between the nozzle and the filament of the drop. This break-up situation for DOD closely resembles the break-up situation with the filament thinning and break-up viewed either above or below the central dotted white line, which represents one plane of symmetry. By considering the top or bottom half of the filament profile obtained from the Trimaster as shown in Fig. 10(a), similar features to the DOD process [Fig. 10(b)] can be identified. In particular the Trimaster break-up, as shown in Fig. 10(a), clearly shows a tail between the central thread and the fluid trapped at the end plates. This is very similar to the tail seen in DOD printing shown in Fig. 10(b) between the main drop filament and the exit nozzle of the DOD printer. The manner of filament break-up for the DOD printer is central to the inkjet performance of the device and it is this aspect that is captured by the Cambridge Trimaster as shown in Fig. 10(a).

In both cases, the formation of a tail indicates an extra force, due to the viscoelasticity of the fluid, acting against the break-up by increasing the break-up time. Consequently, the viscoelasticity of the fluid can be either beneficial or detrimental to the drop formation, depending on which break-up is been considered. A greater viscoelasticity is detrimental at the nozzle plate break-up, as it increases the stretching time, resulting in a thinner and longer droplet thread and, thus, a slower droplet velocity. However, it is beneficial close to the main droplet by increasing the recoiling speed and the break-up time, which helps prevent satellite formation.

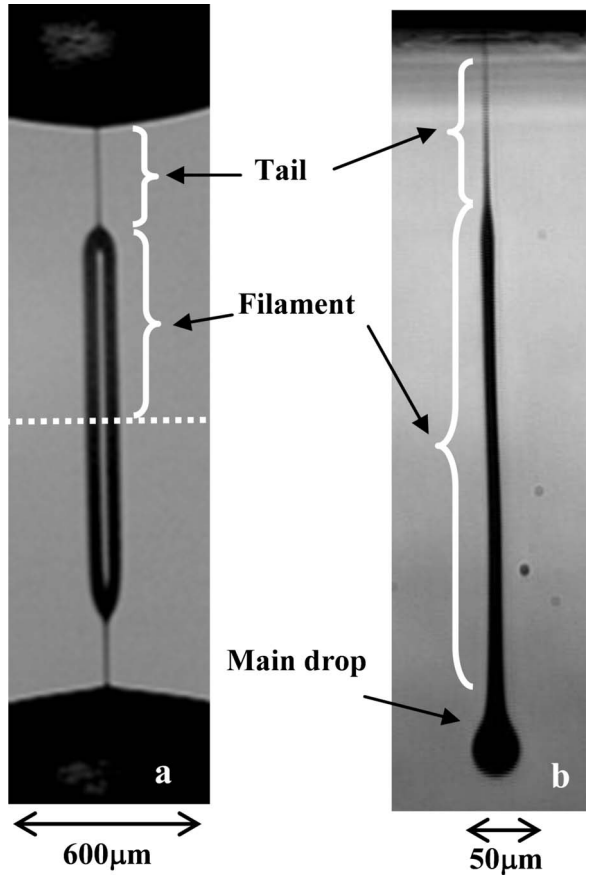

FIG. 10. (a) Trimaster experiment, initial gap size 600 μm, stretching distance 1600 μm, and piston velocity 150 mm/s. (b) Ejection of droplet by DOD (Vadillo, 2007). Central dotted line represents the central symmetry of the filament.

As outlined in Fig. 10, the DOD break-up process involves a wide range of possibilities for both the tail and the thinning filament behind the main drop. This also applies to the Cambridge Trimaster break-up where differences in both main central filament and connecting tail occur. Figure 11 shows the classic range of filament formation as observed in the Cambridge Trimaster where for the Newtonian case in Fig. 11(a) end pinching dominates the break-up (De=0). In Fig. 11(b), a highly viscoelastic fluid shows exponential thinning behavior resulting in a long surviving central thread. A characteristic time scale for viscoelastic stress relaxation in a uni-axial surface tension driven filament thinning elongational flow can then be extracted using the following equation [Liang and Mackley (1994); Rodd *et al.* (2005)]:

$$\frac{D_{mid}(t)}{D_0} = \beta \exp\left(-\frac{t}{3\lambda}\right), \tag{4}$$

where β is a coefficient dependant on the fluid viscosity, the cylindrical thread diameter, and the fluid surface tension. The fluid relaxation has been estimated at 0.43 ms corresponding to a Deborah number De=0.16. An inkjet fluid with an "optimum" viscoelasticity is shown in Fig. 11(c) and gives a well defined stable central filament with short living tails.

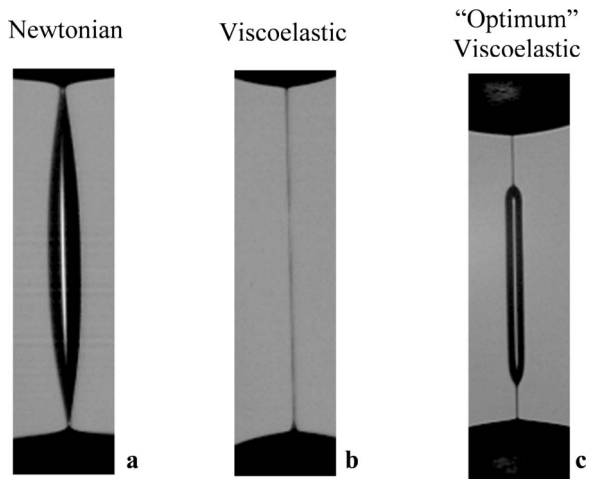

FIG. 11. General schematic at the break-up for (a) Newtonian fluid, (b) non-Newtonian fluid with high viscoelasticity, and (c) non-Newtonian but expected to be the optimum. Initial gap: 600 μm; stretching distance: 1600 μm; piston velocity: 150 mm/s; capture frequency: 27 000 fps.

The optimum break-up behavior for a DOD drop is a very subtle balance in relation to trailing filament formation and break-up. This is illustrated in Fig. 10(b) where the ideal situation would be that break-up occurs at the tail and subsequently the trailing filament retracts back into the main drop thereby not forming unwanted satellites, as schematically described in Figs. 9(d) and 9(l). The Cambridge Trimaster filament thinning and break-up profile associated with this optimum fluid viscoelasticity is given in Fig. 11(c). If end pinching occurs at both ends of the filament during filament thinning [Fig. 11(a)], a central droplet is formed. In terms of jetting, it schematically corresponds to the path 1 of Fig. 9 where the filament may break-up into one satellite drop [Fig. 9(f)]. If the filament thinning break-up is delayed too long [Fig. 11(b)], there is potential for forming Rayleigh instabilities along the trailing thread which subsequently breaks up into satellite drops, as schematically shown in Figs. 9(h) and 9(m). Finally, if the fluid is too viscoelastic, the consequent inkjet drop profile would be a filament which (i) stretches without break-up, (ii) retracts into the jetting device, or (iii) cannot be released from the printhead.

According to the Cambridge Trimaster profiles in Fig. 3, for the mixture of DEP and PS110, the ideal polymer weight concentration for a DOD fluid for the purposes of jetting is between 0.2 and 0.5 wt %. In these cases, the filament profiles obtained during filament thinning experiments exhibit a break-up with the formation of a droplet and a tail. In contrast, the DEP with 0.01 wt % of PS110, which behaves as a Newtonian fluid, is expected to form satellites. When the concentration of PS110 was higher than 1 wt %, where the filament lifetime was long, the fluid is not expected to be particularly jettable and to form a filament which is too long, i.e., the filament has not recoiled into the main droplet before impact. With even greater polymer concentrations, the drop will be drawn back into the printhead after it is ejected and thus be not jettable. These hypotheses have been confirmed by the jetting of the fluid presented in this study as well as separate studies [Bazilevsky *et al.* (2005); Xu *et al.* (2007); Hoath *et al.* (2008)]. The fluids have been jetted by a Xaar XJ 126–200 DOD printhead at 6 m/s by adapting the amplitude of the wave form but conserving the pulse width to correct the viscosity enhancement of the solution with the addition of polymer and photographs of the droplet formation are presented Fig. 12. The satellite formation has been reduced between the DEP with

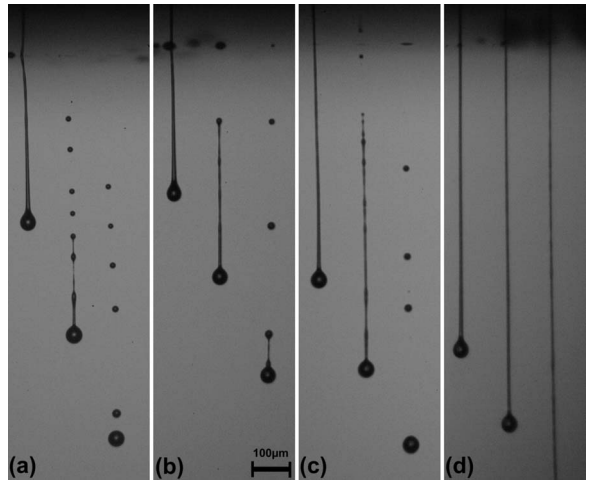

FIG. 12. Photographs of the DOD droplet formation mechanism for (a) DEP+0.01 wt % PS110, (b) DEP +0.2 wt % PS110, (c) DEP+0.5 wt % PS110, and (d) DEP+1 wt % PS110. The droplets were generated at 6 m/s using a Xaar XJ 126-200 printhead. Nozzle diameter of 50 μm, the spatial and time intervals between the droplets on each picture are 137 μm and 56 μs, respectively.

0.01 wt % of PS110 [Fig. 12(a)] and the DEP loaded with 0.2–0.5 wt % of monodisperse PS [Figs. 12(b) and 12(c)]. A small difference can also be seen between the DEP solution loaded with 0.2 and 0.5 wt % PS110. Increasing the polymer loading caused the elongation of the drop threads resulting in a higher distance between the satellites and the main droplet as well as the formation of mist droplets [Figs. 12(b) and 12(c)]. Figure 12(b) shows two satellites with a third one under formation but this catches up the main droplet later, resulting in the formation of a maximum of two satellites. Figure 12(c) shows three satellites and the presence of a very small drop, named a mist drop, located between the second and the third satellites. In DOD inkjet printing, mist ink drops are undesirable. In continuous inkjet, mist drops create a build-up on the deflection plate and

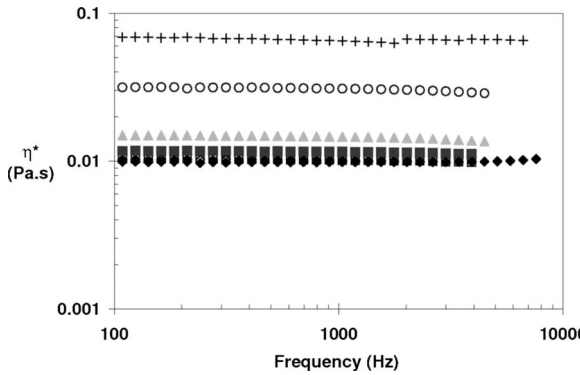

FIG. 13. Complex viscosity η^* of solution of DEP-PS 110k at different concentration. (♦) DEP, (□) DEP −0.1% PS, (×) DEP−0.2% PS, (■) DEP−0.5 wt % PS, (▲) DEP−1 wt % PS, (○) DEP−2.5 wt % PS, (+) DEP−5 wt % PS.

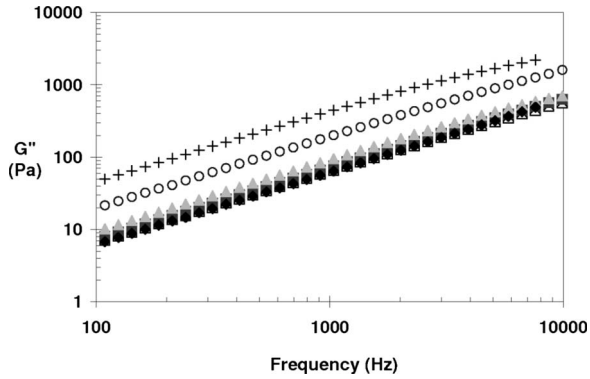

FIG. 14. Viscous modulus G″ of solution of DEP-PS 110k at different concentration. (♦) DEP, (□) DEP −0.1% PS, (×) DEP−0.2% PS, (■) DEP−0.5 wt % PS, (▲) DEP−1 wt % PS, (○) DEP−2.5 wt % PS, (+) DEP−5 wt % PS.

again are undesirable. At even higher concentration (>1 wt %), the fluid was found to be difficult to jet with the formation of a very long drop filament [Fig. 12(d)], making it unsuitable for inkjet printing applications.

V. CONCLUSION AND FURTHER WORK

This paper has presented a new filament stretcher apparatus which enables filament stretching, filament self-thinning, and break-up experiments to be carried out on low viscosity fluids in the range of $\eta_0 = 10$ mPa s. The displacement of the piston is mechanically demanding and the two pistons need to move accurately and at the same speed. The paper has shown that, in a certain velocity range, good piston control has been achieved, however further development is necessary for piston velocities exceeding 300 mm/s. The Cambridge Trimaster is not equipped with a force transducer which would enable the extensional viscosity to be measured during filament stretching experiment; however, capillary self-thinning experiments were performed in order to determine the transient extensional viscosity and the results obtained are consistent with the literature.

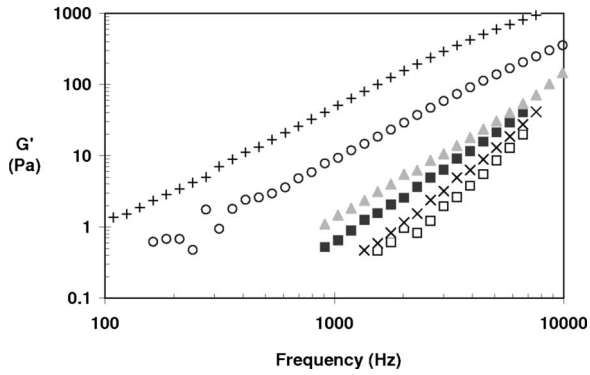

FIG. 15. Elastic modulus G′ of solution of DEP-PS 110k at different concentration. (♦) DEP, (□) DEP −0.1% PS, (×) DEP−0.2% PS, (■) DEP−0.5 wt %, (▲) DEP−1 wt % PS, (○) DEP−2.5 wt % PS, (+) DEP−5 wt % PS.

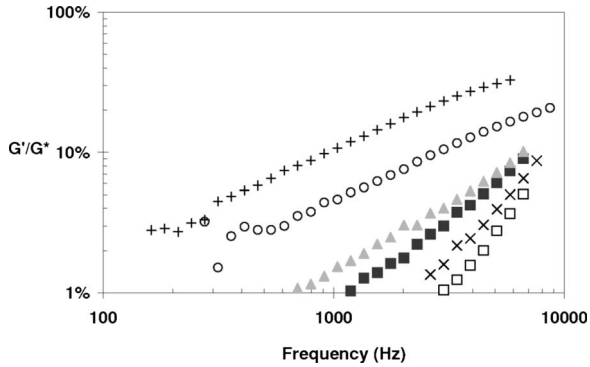

FIG. 16. Elastic ratio G'/G^* of solution of DEP-PS 110k at different concentration. (♦) DEP, (□) DEP −0.1% PS, (×) DEP−0.2% PS, (■) DEP−0.5 wt % PS, (▲) DEP−1 wt % PS, (○) DEP−2.5 wt % PS, (+) DEP−5 wt % PS.

The apparatus enables the determination of filament break-up after a controlled stretch and deformation. Three regimes have been identified: end pinching Newtonian drop formation, viscoelastic filament thinning, and intermediate Rayleigh filament break-up forming small satellites.

The break-up behavior observed using the Cambridge Trimaster has then been compared to DOD drop break-up behavior and several linking factors identified. Useful information on DOD break-up can therefore be obtained from the Cambridge Trimaster where the initial boundary conditions are in principle simpler than DOD nozzle ejection and viscoelastic numerical simulation can be carried out in order to test viscoelastic break-up models with experimental observations. Capillary self-thinning experiments were performed in order to determine the transient extensional viscosity and some results obtained are consistent with the filament thinning results obtained by Tuladhar and Mackley (2008) using the MPR filament thinning configuration.

ACKNOWLEDGMENTS

This work was supported by the UK Engineering and Physical Sciences Research Council (EPSRC) and by a consortium of industrial partners within the Cambridge Inkjet Research Centre through Grant No. GR/T11920/01. Professor Ian Hutchings and Dr. Graham Martin from the Institute for Manufacturing at the University of Cambridge are acknowledged for their technical support. The authors also want to acknowledge Surinder Sall and Lee Pratt for their involvement in the development of the Trimaster.

APPENDIX

Rheological characterization of the fluid used in the study is shown in Figs. 13–16. The linear viscoelasticity is measured using a piezo axial vibrator [Groß *et al.* (2002); Crassous *et al.* (2005)].

References

Anna, S. L., and G. H. McKinley, "Elasto-capillary thinning and breakup of model elastic liquids," J. Rheol. **45**, 115–138 (2001).

Anna, S. L., C. Rogers, and G. H. McKinley, "On controlling the kinematics of a filament stretching rheometer

using a real-time active control mechanism," J. Non-Newtonian Fluid Mech. **87**, 307–335 (1999).

Bach, A., H. Koblitz Rasmussen, and O. Hassager, "Extensional viscosity for polymer melts measured in the filament stretching rheometer," J. Rheol. **47**(2), 429–441 (2003).

Bach, A., H. K. Rasmussen, P. Y. Longin, and O. Hassager, "Growth of non-axisymmetric disturbances of the free surface in the filament stretching rheometer: Experiments and simulation," J. Non-Newtonian Fluid Mech. **108**, 163–186 (2002).

Bazilevsky, A. V., V. M. Entov, and A. N. Rozhkov, "Failure of polymer solutions filaments," Polym. Sci., Ser. A Ser. B **39**, 316–324 (1997).

Bazilevsky, A. V., J. D. Meyer, and A. N. Rozhkov, "Dynamics and breakup of pulse microjets of polymeric liquids," Fluid Dyn. **40**(3), 376–392 (2005).

Bazilevsky, A. V., V. M. Entov, and A. N. Rozhkov, "Liquid filament microrheometer and some of its applications," *Third European Rheological Conference*, edited by D. R. Oliver (Elsevier Applied Science, 1990), 41–43.

Brenner, M. P., J. R. Lister, and H. A. Stone, "Pinching threads, singularities and the number 0.0304," Phys. Fluids **8**, 2827–2836 (1996).

Clasen, C., J. P. Plog, W.-M. Kulicke, M. Owens, C. Macosko, L. E. Scriven, M. Verani, and G. H. McKinley, "How dilute are dilute solutions in extensional flows?," J. Rheol. **50**(6), 849–881 (2006).

Crassous, J., R. Régisser, M. Ballauff, and N. Willenbacher, "Characterization of the viscoelastic behavior of complex fluids using the piezoelastic axial vibrator," J. Rheol. **49**, 851–863 (2005).

Dong, H., W. W. Carr, and J. F. Morris, "An experimental study of drop-on-demand drop formation," Phys. Fluids **18**, 072102 (2006).

Eggers, J., "Nonlinear dynamics and breakup of free-surface flows," Rev. Mod. Phys. **69**, 865–929 (1997).

Entov, V. M., and E. J. Hinch, "Effect of a spectrum relaxation times on the capillary thinning of a filament elastic liquids," J. Non-Newtonian Fluid Mech. **72**, 31–53 (1997).

Graessley, W. W., "Polymer chain dimensions and the dependence of viscoelastic properties on the concentration, molecular weight and solvent power," Polymer **21**, 258–262 (1980).

Groß, T., L. Kirschenmann, and W. Pechhold, "Piezo axial vivrator (PAV)—A new oscillating squeeze flow rheometer," Proceedings Eurheo, edited by H. Munsted, J. Kaschta, and A. Merten, Erlangen (2002).

Hoath, S. D., G. D. Martin, I. M. Hutchings, T. R. Tuladha, and M. R. Mackley, "Links between fluid rheology and drop-on-demand jetting and printability (focal)," Final Program and Proceedings of IST&T's NIP 24, Pittsburgh, 2008, Vol. 24.

Hoath, S. D., G. D. Martin, T. R. Tuladhar, M. R. Mackley, D. Vadillo, and I. Hutching, "Link between ink rheology, drop-on-demand jet formation and printability," J. Imaging Sci. Technol. **53**, 041208 (2009).

Hutchings, I. M., G. D. Martin, and S. D. Hoath, "High speed imaging and analysis of jet and drop formation," J. Imaging Sci. Technol. **51**(5), 438–444 (2007).

Jang, D., D. Kim, and J. Moon, "Influence of fluid physical properties on ink-jet printability," Langmuir **25**, 2629–2635 (2009).

Kolte, M. I., and P. Szabo, "Capillary thinning of polymeric filaments," J. Rheol. **43**, 609–625 (1999).

Liang, R. F., and M. R. Mackley, "Rheological characterisation of the time and strain dependence for polyisobutylene solutions," J. Non-Newtonian Fluid Mech. **52**, 387–405 (1994).

Ma, W. K. A., F. Chinesta, T. Tuladhar, and M. R. Mackley, "Filament stretching of carbon nano tube suspension," Rheol. Acta **47**, 447–457 (2008).

Mackley, M. R., R. T. J. Marshall, and J. B. A. Smeulders, "The multipass rheometer," J. Rheol. **39**(6), 1293–1309 (1995).

Matta, J. E., and R. P. Tytus, "Liquid stretching using falling cylinder," J. Non-Newtonian Fluid Mech. **35**, 215–229 (1990).

McKinley, G. H., "Visco-elastic-capillary thinning and break-up of complex fluid," *Rheology Reviews 2005* (The British Society of Rheology, 2005), pp. 1–49.

McKinley, G. H., and T. Sridhar, "Filament stretching rheometry of complex fluids," Annu. Rev. Fluid Mech. **34**, 375–415 (2002).

McKinley, G. H., and A. Tripathi, "How to extract the Newtonian viscosity from capillary breakup measurements in a filament rheometer," J. Rheol. **44**, 653–670 (2000).

Orr, N. V., and T. Sridhar, "Probing the dynamics of polymer solutions in extensional flow using step strain rate experiments," J. Non-Newtonian Fluid Mech. **82**, 203–232 (1999).

Papageorgiou, D. T., "On the breakup of viscous liquid threads," Phys. Fluids **7**, 1529–1544 (1999).

Renardy, M., "Some comments on the surface tension driven breakup (or the lack of it) of the viscoelastic jets," J. Non-Newtonian Fluid Mech. **51**, 97–107 (1994).

Renardy, M., "A numerical study of the asymptotic evolution and breakup of Newtonian and viscoelastic jets," J. Non-Newtonian Fluid Mech. **59**, 267–282 (1995).

Rodd, L. E., T. P. Scott, J. J. Cooper-White, and G. H. McKinley, "Capillary breakup rheometry of low-viscosity elastic fluids," Appl. Rheol. **15**(1), 12–27 (2005).

Spiegelberg, S. H., D. C. Ables, and G. H. McKinley, "The role of end-effects on measurements of extensional viscosity in filament stretching rheometers," J. Non-Newtonain Fluid Mech. **64**, 229–267 (1996).

Sridhar, T., "An overview of the project M1," J. Non-Newtonain Fluid Mech. **35**, 85–92 (1990).

Sridhar, T., V. Tirtaatmadja, D. A. Nguyen, and R. K. Gupta, "Measurement of extensional viscosity of polymer solutions," J. Non-Newtonain Fluid Mech. **40**, 271–280 (1991).

Stelter, M., G. Brenn, A. L. Yarin, R. B. Singh, and F. Durst, "Validation and application of a novel elongation device for polymer solutions," J. Rheol. **44**, 595–616 (2000).

Tuladhar, T. R., and M. R. Mackley, "Filament stretching rheometry and break-up behaviour of low viscosity polymer solutions and ink jets fluids," J. Non-Newtonain Fluid Mech. **148**, 97–108 (2008).

Vadillo, D. C., Ph.D. thesis, Grenoble, 2007.

Weinberger, G. B., and J. D. Goddard, "Extensional flow behaviour of polymer solutions and particles suspension in spinning motion," Int. J. Multiphase Flow **1**, 465–486 (1974).

Xu, D., V. Sanchez-Romaguera, S. Barbosa, W. Travis, J. De Wit, P. Swan, and S. G. Yeates, "Inkjet printing of polymer solutions and the role of chain entanglement," J. Mater. Chem. **17**, 4902–4907 (2007).